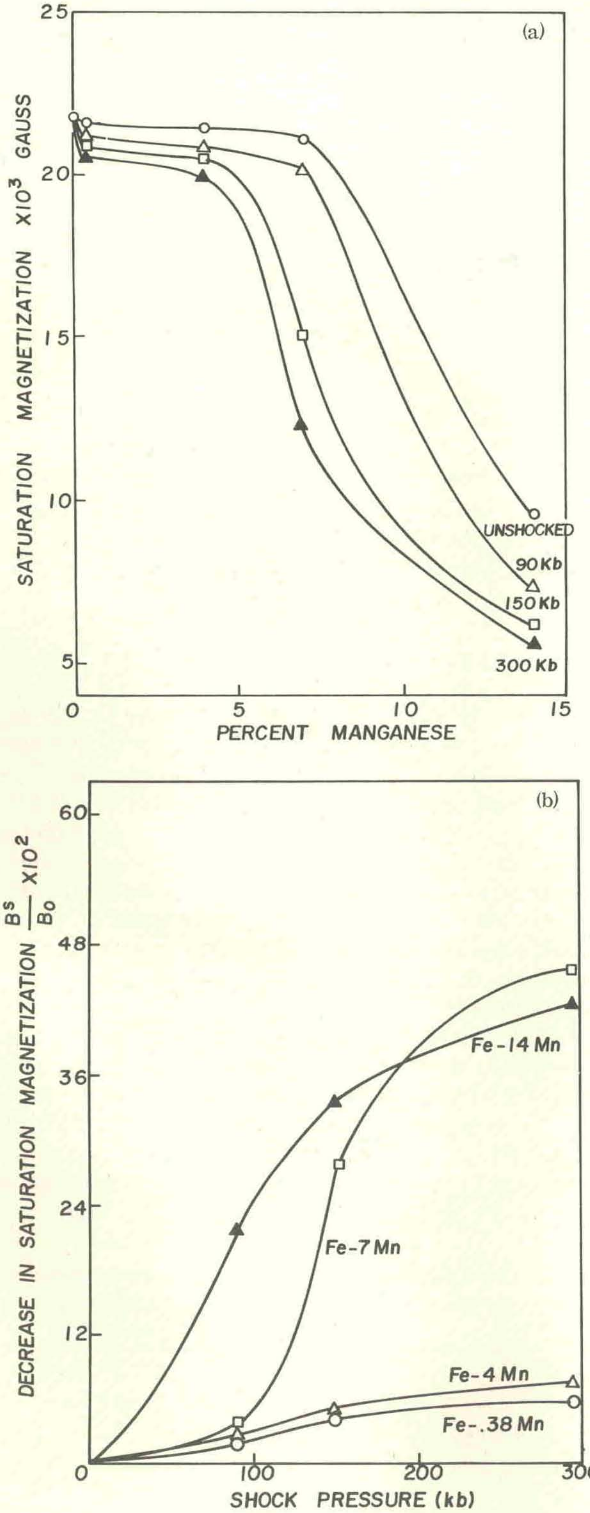

FIG. 10. (a) Saturation magnetization as a function of manganese content for shocked and unshocked alloys. (b) Fractional change in saturation magnetization as a function of peak pressure.

direction and are aligned along the $[110]_{bcc}$. The diffraction pattern of Fig. 7(b) (Fe-7Mn, 300 kbar) is primarily fcc; and, when the bcc and fcc diffraction patterns are superimposed, the following crystallo-

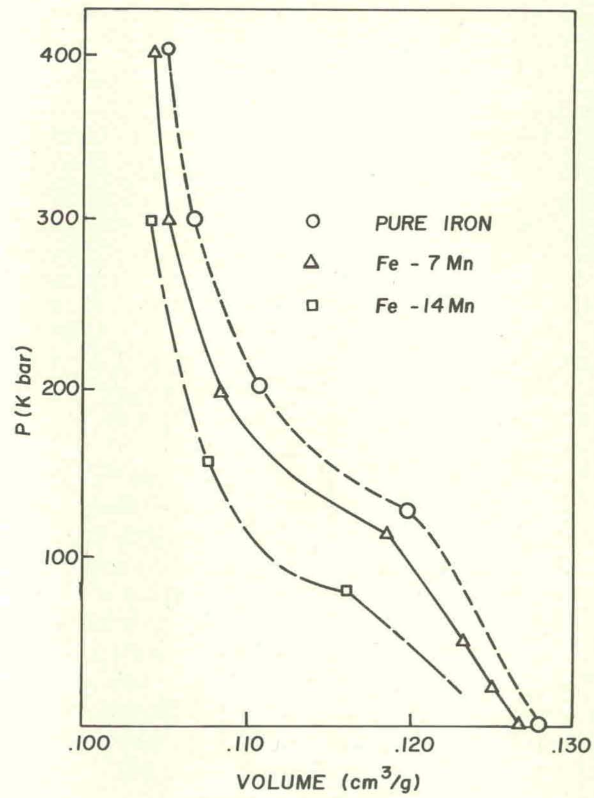

FIG. 11. Hugoniot curves for Fe-Mn alloys.

graphic relationship was obtained:

$$[\bar{1}11]_{\gamma} \| [110]_{m}, \quad (101)_{\gamma} \| (\bar{1}1\bar{1})_{m}. \tag{1}$$

This orientation relationship corresponds to that of Kurdjumov and Sachs.

The habit plane of the fcc phase in shocked Fe-7Mn was determined by single surface trace analysis. Two different types of habit planes were observed at 90 kbar. Five habits were approximately $(\bar{1}\bar{1}2)_{\gamma}$ and only one was near $(\overline{2}\overline{2}5)_{\gamma}$. At 150 kbar, for the variant of the orientation relationship used, the habit plane was always found to be near $(\bar{1}\bar{1}2)_{\gamma}$.

D. Magnetization Measurements

The magnetization curves appearing in Fig. 9 indicate different approaches to saturation at each pressure. In general there is a lowering of saturation magnetization with increasing shock pressure, as shown in Fig. 10(a). The fractional decrease in saturation magnetization is shown in Fig. 10(b). The greatest fractional change in saturation magnetization occurred for the Fe-7Mn alloy, which was shocked at 300 kbar. However, at 150 kbar the change in saturation magnetization was greater for the Fe-14Mn than for the Fe-7Mn alloy. This observation is consistent with the density measurements. Figure 10(a) shows that the saturation magnetization changes only slightly with shock pressure when the manganese content is below 4 wt%. This means that the change in the *B-H* curve produced by dislocations is relatively small compared to the change produced

TABLE IV. Retained high-pressure phases of the quenched alloys.

Alloy	Pressure (kbar)	Vol% fcc Density	Vol% fcc Magnetization	Vol% hcp Density	Vol% hcp Magnetization
Fe-4Mn	90	2.25	3.10		
	150	10.80	6.50		
	300	16.25	11.00		
	500	15.50	13.50		
Fe-7Mn	90	3.12	3.20		
	150	25.25	24.00		
	300	47.50	45.00		
	500	47.60	47.00		
Fe-14Mn	90			30.10	25.00
	150			38.00	34.50
	300			49.20	44.00
	500			49.20	45.00

by the retention of the close-packed paramagnetic phases. For the Fe-7Mn alloy, as shown in Fig. 10(a), and decrease in saturation magnetization between 90 and 150 kbar is the result of the $\alpha' \rightarrow \gamma$ transformation. In the Fe-14Mn alloy, a significant decrease in saturation magnetization occurs below 90 kbar. It is likely that the transformation was initiated below 90 kbar for the Fe-14Mn alloy. The decrease is saturation magnetization with shock pressure for the Fe-14Mn alloy is caused by the retention of the close-packed phase.

IV. DISCUSSION

A. Discussion of Experimental Results

The density data, magnetic data, and microstructure all show that close-packed phases can be retained after shock loading if the unshocked specimens contained bcc martensite, with the manganese content in the range 4–16 wt%. Alloys which were slow cooled did not retain the high-pressure phase after shock loading because their bcc martensite contained less than 4 wt% Mn. In addition, the slow-cooled alloys already contained a close-packed phase prior to shock loading. Therefore, manganese in bcc martensite, between 4 and 16 wt% stabilizes the high-pressure close-packed phases. It is of interest to calculate the amount of retained phases based on the different types of measurements.

From the rigid-sphere model, a theoretical density change for $\alpha \rightarrow \gamma$ is 8.98% and for $\alpha \rightarrow \epsilon$ is 9.12%. Using the density measurements of Table II, the percentages of retained high-pressure phases have been calculated as shown in Table IV. The amount of retained high-pressure phases can also be estimated from the magnetization measurements, based on the difference in saturation magnetization between the shocked and unshocked specimens (Table IV). It is to be noted that the estimate of the amount of retained high-pressure phase from the density and magnetic data is the same. Table II shows that all alloys, and even the pure iron, showed an increase in density after shock loading. It would appear that the density changes from 1.0001 to 1.0003 may be a result of microvoid coalescence.[11,12] Possibly the density changes which were observed in the furnace-cooled alloys with 4–14 wt% Mn may be caused by very small amounts of retained high-pressure phases which were not detectable by the other methods of

TABLE V. Retained high-pressure phases in alloys.

Alloy	Heat treatment	Phase transformation	Habit plane and shear system
Fe-32 Wt% Ni (Ref. 20)	LNQ[a]	$\alpha' \rightarrow \gamma$	$\sim (5\bar{2}3)\alpha$ $(110)\gamma\ [1\bar{1}0]\gamma$
Fe-Ni-C (Ref. 20)	LNQ	$\alpha' \rightarrow \gamma$	$(225)\gamma$ $(110)\gamma\ [1\bar{1}0]\gamma$ $(11\bar{2})\gamma$ $(111)\gamma\ [\bar{1}2\bar{1}]\gamma$
Fe-7Mn, Fe-4Mn (present work, Ref. 6)	Water quench	$\alpha' \rightarrow \gamma$	$(\bar{1}\bar{1}2)\gamma$(Fe-7Mn) $(111)\gamma\ [\bar{1}2\bar{1}]\gamma$
Fe-14Mn		$\alpha' \rightarrow \epsilon$	...
Ti-Mo (Ref. 22)	LNQ	$\alpha \rightarrow \epsilon$	...
Ti-V (Ref. 22)	LNQ	$\alpha \rightarrow \epsilon$	...

[a]Liquid-nitrogen quench.